

A BROADBAND MODEL FOR SINGLE-MODE FIBERS INCLUDING NONLINEAR DISPERSION

K. Grobe

Institut für Allgemeine Nachrichtentechnik
Universität Hannover
30167 Hannover, Germany

H. Braunsch

Department of Electrical Engineering and Computer Science
Research Laboratory of Electronics
Massachusetts Institute of Technology
Cambridge, MA 02139, USA

- 1. Introduction**
- 2. Nonlinear Schrödinger Equation**
- 3. Fiber Equations in the Frequency Domain**
- 4. Modeling of Nonlinear Effects**
- 5. Numerical Examples**
- 6. Proposal of an Efficient Bidirectional Algorithm**
- 7. Conclusions**

References

1. INTRODUCTION

There has been an increasing demand for high-capacity fiber-optic transmission systems covering short to ultra-long distances. This has led to a rapid development of new hardware components and transmission technologies. For example, the trans-atlantic systems TAT12/13 provide for bidirectional data transmission of 2×5 Gb/s using intensity modulation and direct detection (IM/DD) techniques and a single-channel configuration [1]. The currently installed system Sea-Me-We-3 will use 4-channel Wavelength-Division Multiplexing (WDM) to

provide for 10 Gb/s with an overall system length spanning 27,000 km [2]. Higher bit rates of 40 Gb/s and beyond can be achieved by either using ultra-short pulses and Optical Time-Division Multiplexing (OTDM) and/or by Optical Frequency-Division Multiplexing (OFDM) with an increased number of channels. OFDM can be divided into Dense WDM (DWDM) and Coherent Multi-Channel (CMC). Examples for DWDM submarine systems are UK-Germany-6 (40 Gb/s, to be installed in 1998) and the trans-atlantic Gemini system (30 Gb/s, to be installed in 1998/99).

OTDM with ultra-short pulses and OFDM lead to large bandwidths. Propagation of signals is then limited by frequency-dependent linear and nonlinear detrimental effects. To calculate these effects correctly an appropriate nonlinear and dispersive model is needed. Commonly, one uses the *Nonlinear Schrödinger Equation* (NLSE) for an analysis of pulse propagation in the time domain [3–6]. The NLSE can be used for pulse widths down to 100 fs and nonlinear dispersion is neglected. A Generalized NLSE (GNLSE) was developed to include effects of stimulated Raman scattering (SRS) [3, 7, 8]. The GNLSE can be used for pulses not shorter than 25 fs.

Since the NLSE can be solved analytically in only very few cases using inverse scattering methods [9, 10], numerical approaches are needed. Two categories exist, namely *pseudo-spectral* and *finite-differences* methods [3]. The NLSE and similar approaches neglect the second derivatives of the signals with respect to the direction of propagation, z . This is called the slowly varying amplitude approximation and leads to numerical solutions using the pseudo-spectral *split-step Fourier algorithm*. If the second derivatives are to be retained, direct solving of Maxwell's equations in the time domain by means of the *Finite-Differences Time-Domain* method (FDTD) is used [11]. This method has been applied in nonlinear optics [12], its disadvantage is a vast requirement of CPU time.

In this paper a broadband fiber model in the frequency domain is presented. This permits convenient modeling of linear and nonlinear dispersion using their frequency-dependent characteristics. In contrast to other models like the GNLSE we use coupled equations for the electric and the magnetic field, respectively. This leads to special nonlinear transmission-line equations, either for fast-varying bandpass signals or for slowly-varying envelopes. These equations can be solved with a fast pseudo-spectral method neglecting the second derivatives with respect

to z , or with a special combination of FDTD and pseudo-spectral methods. As the second derivatives with respect to z are retained backscattering effects caused by mismatch of the wave impedance and Stimulated Brillouin Scattering (SBS) can be described.

2. NONLINEAR SCHRÖDINGER EQUATION

The propagation of pulse-envelopes in optical fibers is usually described by the *Nonlinear Schrödinger Equation* (NLSE) [3–6]. The NLSE contains approximations that limit its use with respect to ultra-broadband signals. The standard form of the NLSE does not contain any frequency-dependence in its nonlinear part and scattering effects are neglected:

$$\frac{\partial e_T}{\partial z} = -\beta_1 \frac{\partial e_T}{\partial t} + \frac{j\beta_2}{2} \frac{\partial^2 e_T}{\partial t^2} - \alpha_0 e_T - \frac{j\beta_0 n_2}{n_0} |e_T|^2 e_T \quad (1)$$

Here, $e_T = e_T(z, t)$ denotes the complex pulse-envelope in the time domain, $\beta_i = \partial^i \beta / \partial \omega^i |_{\omega_0}$ are coefficients of a Taylor expansion of the phase constant $\beta(\omega)$ around a central (carrier) frequency ω_0 , α_0 is the attenuation at ω_0 , and n_0 and n_2 are the linear refractive index at frequency ω_0 and the nonlinear refractive index coefficient, respectively. n_2 is related to the third-order nonlinear susceptibility $\chi_0^{(3)}$ by $n_2 = 3\chi_0^{(3)} / 8n_0$. A special numerical *split-step Fourier algorithm* exists that is a fast and convenient tool for solving the NLSE, making it a powerful model for pulse propagation with limited bandwidth [3]. The NLSE (1) does not include scattering effects as it only contains the frequency-independent nonlinearity n_2 .

To include Stimulated Raman Scattering (SRS), a *Generalized NLSE* can be constructed [3, 7, 8]. SRS is included into the GNLSE by a convolution integral:

$$\begin{aligned} \frac{\partial e_T}{\partial z} = & \sum_{i=1}^3 \beta_i \frac{(-j)^{i+1}}{i!} \frac{\partial^i e_T}{\partial t^i} - \alpha_0 e_T - \frac{j\beta_0 n_2}{n_0} \left(1 + \frac{j}{\omega_0} \frac{\partial}{\partial t} \right) \\ & \cdot \left(e_T(z, t) \int_0^\infty R(\tau) |e_T(z, t - \tau)|^2 d\tau \right) \end{aligned} \quad (2)$$

$R(t)$ includes SRS and the instantaneous Kerr effects Self-Phase Modulation (SPM), Cross-Phase Modulation (XPM) and Four-Wave Mixing (FWM). The *shock term* $(j/\omega_0)(\partial/\partial t)$ accounts for the frequency

dependence of the transverse modal field [7] by means of a truncated Taylor series. The GNLSE neglects SBS, and again a Taylor series is used for modeling (higher order) dispersion in the time domain. The GNLSE (2) cannot be solved with the split-step Fourier algorithm resulting in increased numerical complexity. If these problems are to be circumvented, a full-signal approach in the frequency domain including conservation of momentum should be used.

3. FIBER EQUATIONS IN THE FREQUENCY DOMAIN

The derivation of a model for calculating pulse-envelope propagation in single-mode fibers starts with the source-free Maxwell's equations in the frequency domain:

$$\nabla \times \mathbf{H}(\mathbf{r}, \omega) = j\omega \mathbf{D}(\mathbf{r}, \omega) \quad (3)$$

$$\nabla \times \mathbf{E}(\mathbf{r}, \omega) = -j\omega \mu_0 \mathbf{H}(\mathbf{r}, \omega) \quad (4)$$

with electric and magnetic field vectors \mathbf{E} and \mathbf{H} . Linear and nonlinear dispersion effects are included via the electric displacement $\mathbf{D} = \varepsilon_0 \mathbf{E} + \mathbf{P}$. We now consider linearly polarized vector fields so that equations (3)/(4) and the polarization \mathbf{P} may be reduced to scalar quantities. Nonlinear susceptibilities of even order are negligible due to inversion symmetry [3, 5] of the media considered. Suppressing higher order nonlinearities as well the polarization P can be written as:

$$P(\mathbf{r}, \omega) = \varepsilon_0 X^{(1)}(\mathbf{r}, \omega) E(\mathbf{r}, \omega) + \frac{1}{4\pi^2} \iint_{-\infty}^{\infty} \varepsilon_0 X^{(3)}(\mathbf{r}, \omega_1, \omega_2, \omega_3) \cdot E(\mathbf{r}, \omega_1) E(\mathbf{r}, \omega_2) E(\mathbf{r}, \omega_3) d\omega_1 d\omega_2 \quad (5)$$

where $\omega_3 = \omega - \omega_1 - \omega_2$. The susceptibility $X^{(1)}(\omega) = n^2(\omega) - 1$ is responsible for (linear and higher order) dispersion and can be described by the Sellmeier series [3]:

$$n^2(\omega) = 1 + \sum_{i=1}^3 \frac{B_i \omega_i^2}{\omega_i^2 - \omega^2} \quad (6)$$

In equation (6), the resonance frequencies and their weighting coefficients are: $B_1 = 0.6961663$, $\lambda_1 = 0.0684043 \mu\text{m}$, $B_2 = 0.4079426$, $\lambda_2 = 0.1162414 \mu\text{m}$, and $B_3 = 0.8974794$, $\lambda_3 = 9.8961610 \mu\text{m}$. The

Sellmeier series provides for an ultra-broadband description of dispersion in the frequency domain. Next, appropriate expressions for the transverse field of the fundamental mode must be inserted [6]. This will introduce the frequency-dependent effects of wave guidance to our model. Combining these with $X^{(1)}$ and $X^{(3)}$ of bulk silica as used in (5) leads to *effective* system parameters $X_{\text{eff}}^{(1)}(\omega)$, $n_{\text{eff}}^2(\omega)$, and $X_{\text{eff}}^{(3)}(\omega_1, \omega_2, \omega_3)$ which consider material and wave-guiding effects in an inherently broadband way.

Inserting the transverse modal distribution in weakly guiding fibers, Maxwell's equations can be reduced to one spatial dimension (i.e., the direction of propagation z). Using effective system parameters the following pair of coupled equations in the frequency domain can be derived:

$$\begin{aligned} \frac{\partial}{\partial z} E(z, \omega) &= j\omega \mu_0 H(z, \omega) & (7) \\ \frac{1}{j\omega} \frac{\partial}{\partial z} H(z, \omega) &= \varepsilon_0 n_{\text{eff}}^2(\omega) E(z, \omega) + \frac{\mu_0}{4\pi^2 n_{\text{eff}}^2(\omega)} \iint_{-\infty}^{\infty} X_{\text{eff}}^{(3)}(\omega_1, \omega_2, \omega_3) \\ &\quad \cdot H(z, \omega_1) H(z, \omega_2) E(z, \omega_3) d\omega_1 d\omega_2 & (8) \end{aligned}$$

Equations (7)/(8) are found in [13], where they are referred to as the *nonlinear fiber equations*. They are cubic nonlinear transmission-line equations, adapted to the characteristics of signal propagation in (single-mode) optical fibers. Note that the integrand in (8) contains both, E and H . This leads to the conservation of momentum even in the nonlinear part of (8). To prove this property, one has to consider the total energy $W(z)$ propagating along the fiber:

$$W(z) = \frac{1}{\pi} \int_{-\infty}^{\infty} \int_0^{\infty} \int_0^{2\pi} \frac{1}{2} \text{Re} \{ \mathbf{E}(\mathbf{r}, \omega) \times \mathbf{H}^*(\mathbf{r}, \omega) \} \cdot \mathbf{z} \rho d\varphi d\rho d\omega \quad (9)$$

where $\mathbf{z}, \rho, \varphi$ are cylindrical coordinates. Necessary for conservation of momentum is that the transmitted energy be constant in the direction of propagation, i.e., $dW(z)/dz = 0$. Neglecting attenuation for the moment and inserting the fiber equations (7)/(8) into (9) gives the following condition for the phase constants:

$$\beta(\omega) - \beta(\omega_1) + \beta(\omega_2) - \beta(\omega_3) = 0 \quad (10)$$

Considering the signs of the phase constants (i.e., the wave vectors), equation (10) is identical to the conservation law of momentum and, for example, describes the relationship between wave vectors in Brillouin scattering. As a consequence of this the fiber equations (7)/(8) can be used to calculate backscattering effects. This holds as long as the momentum of the excited phonons is taken into account. Otherwise (7)/(8) like the GNLSE provide for the conservation of the total photon number [8].

Equations (7)/(8) are valid for any given z -dependent real band-pass signals. In order to obtain a numerically efficient algorithm it is important to separate the carrier wave and to introduce complex pulse-envelopes. To simplify calculations it is necessary to restrict the considered frequencies to one octave of bandwidth centered about a central (carrier) frequency ω_0 , i.e., $E(\omega) = 0$ for $|\omega - \omega_0| \geq \Omega$ and $\Omega \leq \omega_0/2$. This corresponds to a maximum wavelength range 670...2000 nm which imposes no serious limitation on our broadband fiber model.

If complex pulse-envelope spectra

$$E_T(z, \omega) := \begin{cases} 2 E(z, \omega + \omega_0) e^{jk_0 z} & |\omega| < \Omega \\ 0 & |\omega| \geq \Omega \end{cases} \quad (11)$$

are introduced to the nonlinear fiber equations (7)/(8), this yields:

$$\frac{\partial}{\partial z} E_T(z, \omega) = jk_0 E_T(z, \omega) + j(\omega + \omega_0) \mu_0 H_T(z, \omega) \quad (12)$$

$$\begin{aligned} \frac{\partial}{\partial z} H_T(z, \omega) &= j(\omega + \omega_0) \varepsilon_0 n_{\text{eff}}^2(\omega + \omega_0) E_T(z, \omega) \\ &+ jk_0 H_T(z, \omega) + e^{-2\alpha_0 z} K_T(z, \omega) \end{aligned} \quad (13)$$

where

$$\begin{aligned} K_T(z, \omega) &:= \frac{j(\omega + \omega_0) \mu_0}{16 \pi^2 n_{\text{eff}}^2(\omega + \omega_0)} \\ &\cdot \iint_{-\Omega}^{\Omega} 2 X_{\text{eff}}^{(3)}(\omega_1 + \omega_0, -\omega_2 - \omega_0, \omega + \omega_0 - \omega_1 + \omega_2) \\ &\cdot H_T(z, \omega_1) H_T^*(z, \omega_2) E_T(z, \omega - \omega_1 + \omega_2) \\ &+ X_{\text{eff}}^{(3)}(\omega_1 + \omega_0, \omega_2 + \omega_0, \omega - \omega_0 - \omega_1 - \omega_2) \\ &\cdot H_T(z, \omega_1) H_T(z, \omega_2) E_T^*(z, -\omega + \omega_1 + \omega_2) d\omega_2 d\omega_1 \end{aligned} \quad (14)$$

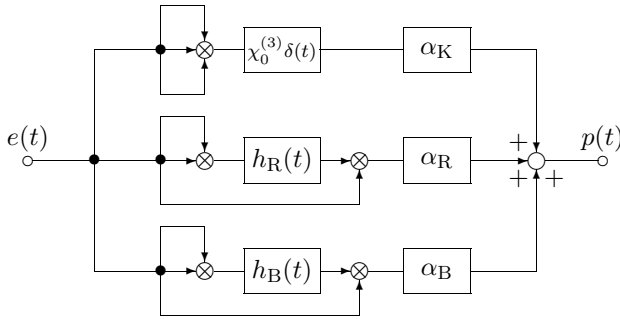


Figure 1. Nonlinear system $e(t) \rightarrow p(t)$.

k_0 is the wave number at frequency ω_0 , and the asterisk denotes complex conjugation. Equations (12)/(13) together with (14) provide a description of pulse-envelope propagation in single-mode fibers including linear and nonlinear dispersion and backscattering effects. They can be used to model any of the linear and nonlinear effects without practical limitations concerning bandwidth.

4. MODELING OF NONLINEAR EFFECTS

Nonlinear effects in optical fibers are well documented, e.g., [3, 5, 14–16]. SPM, XPM, and FWM can be described by a constant Kerr coefficient $X_{\text{Kerr}}^{(3)}(\omega_1, \omega_2, \omega_3) = X^{(3)}(\omega_0, \omega_0, \omega_0) = \chi_0^{(3)} = 3.5 \cdot 10^{-20} \text{ m}^2/\text{V}^2$ [17]. This approximation is valid since the corresponding pulse response decays within 1 fs [8, 18]. In the time domain this corresponds to the product of three delta functions, $\chi_{\text{Kerr}}^{(3)}(t_1, t_2, t_3) = \chi_0^{(3)} \delta(t_1) \delta(t_2) \delta(t_3)$.

The corresponding polarization $p_{\text{Kerr}}(t)$ can be considered as the upper part of the nonlinear polarization $p(t)$ in Fig. 1 which shows a block model of the nonlinear system. The coefficients α_K , α_R , and α_B are adjusted for energy conservation. Their exact values must be fitted to measured data.

Stimulated Raman scattering has its origin in molecular vibrations. Its intensity-dependent susceptibility has the form $\chi_{\text{SRS}}^{(3)}(t_1, t_2, t_3) = \hat{\chi}^{(3)} h_R(t_1, t_2) \delta(t_3)$. Here, $\hat{\chi}^{(3)}$ is a weighting coefficient, and h_R is a normalized response function where $\int h_R(t_1, t_1) dt_1 = 1$. The resulting

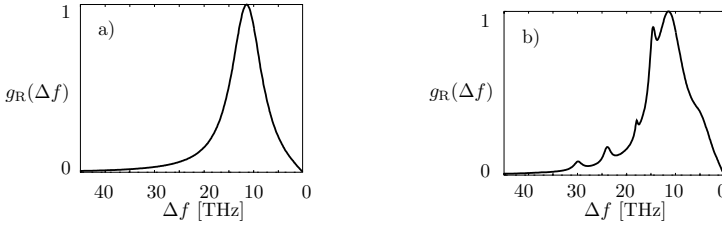


Figure 2. Normalized Raman gain: a) single Lorentzian approximation, b) computed by modified Sellmeier series (17).

Raman polarization is:

$$p_{\text{SRS}}(t) = \varepsilon_0 \hat{\chi}^{(3)} e(t) \int_{-\infty}^t h_{\text{R}}(t_1, t_1) e^2(t - t_1) dt_1 \quad (15)$$

In equation (15) the square of the electric field is convolved by the Raman response function $h_{\text{R}}(t_1, t_1)$ and then multiplied with the electric field again. This is shown in the middle part of Fig. 1.

The Raman susceptibility $X_{\text{SRS}}^{(3)}$ can be derived from the measured Raman gain $g_{\text{R}}(\Delta\omega)$ [3, 8]. This Raman gain is proportional to the imaginary part of the Raman susceptibility,

$$g_{\text{R}}(\Delta\omega) \propto \text{Im}\{X_{\text{SRS}}^{(3)}(\Delta\omega)\}$$

The real part of $X^{(3)}$ must be calculated from the imaginary part through Hilbert transform to guarantee causality. If we combine Raman and wave-guiding effects, we obtain an effective Raman susceptibility:

$$\begin{aligned} X_{\text{SRS}}^{(3)}(\omega_1, \omega_2, \omega_3) &= X_{\text{SRS}}^{(3)}(\Delta\omega) \\ &= \frac{\beta_0 n_0^2}{2 Z_{\text{eff}}(\omega_0)} \frac{\int_0^\infty R_t^4(\rho, \omega_0) \rho d\rho}{\int_0^\infty R_t^2(\rho, \omega_0) \rho d\rho} \left[jg_{\text{R}}(\Delta\omega) + \mathcal{H}\{g_{\text{R}}(\Delta\omega)\} \right] \end{aligned} \quad (16)$$

where Z_{eff} is the wave impedance of the fiber, R_t describes the transverse modal distribution [13], and \mathcal{H} denotes the Hilbert transform. The Stokes shift $\Delta\omega$ is given by $\Delta\omega = \omega - \omega_1$.

It is customary to approximate the Raman frequency response g_R by a single Lorentzian [3, 7, 8]. The Lorentzian is fitted to the main resonance of the gain curve and neglects further resonances, see Fig. 2a. The maximum of the gain curve is given for a Stokes shift of $\Delta f \approx 13$ THz, where $g_R \approx 10^{-13}$ m/W [16].

For a more detailed description of the Raman susceptibility, we choose a specially modified Sellmeier series instead of a single Lorentzian:

$$X_{\text{SRS}}^{(3)}(\Delta\omega) = \sum_{i=1}^6 \frac{b_i}{1 - \left(\frac{\Delta\omega}{\Omega_i}\right)^2 + j \frac{\Delta\Omega_i}{\Omega_i} \frac{\Delta\omega}{\Omega_i}} \quad (17)$$

Here, $\Delta\Omega_i$ is the spectral full-width at half-maximum (FWHM) of the corresponding resonance. The frequencies $\Omega_i/2\pi$ and their coefficients b_i result from curve fitting to $g_R(\Delta\omega)$, their values are summarized in Tab. 1.

The Raman gain as modeled by equation (17) and Tab. 1 is shown in Fig. 2b.

$\Omega_i/2\pi$ [THz]	5.5	12.1	14.7	18.2	24.2	30.3
b_i [m ² /V ²]	2.65	8.90	0.50	0.05	0.11	0.05
$\Delta\Omega_i/2\pi$ [THz]	5.6	7.5	1.4	0.7	1.8	2.0

Table 1. Coefficients of the modified Sellmeier series.

Stimulated Brillouin scattering arises from density fluctuations inside optical fibers caused by electrostriction. The corresponding Brillouin susceptibility $\chi_{\text{SBS}}^{(3)}$ can be modeled in a similar way to $\chi_{\text{SRS}}^{(3)}$ as both are functions of intensity. The Brillouin gain is proportional to the imaginary part of the susceptibility,

$$g_B(\Delta\omega) \propto \text{Im} \{X_{\text{SBS}}^{(3)}(\Delta\omega)\}$$

The Brillouin susceptibility can formally be obtained from (16) by replacing $X_{\text{SRS}}^{(3)}$ and g_R with $X_{\text{SBS}}^{(3)}$ and g_B . The measured Brillouin gain can also be approximated by a Lorentzian spectral profile [3]:

$$g_B(\Delta\omega) = \frac{(\Delta\omega_B/2)^2}{(\Delta\omega - \omega_B)^2 + (\Delta\omega_B/2)^2} g_B(\omega_B) \quad (18)$$

$\Delta\omega_B < 100$ MHz is the spectral FWHM, $\omega_B/2\pi = f_B \approx 11$ GHz is the Stokes shift, and $g_B(\omega_B) \approx 4 \cdot 10^{-11}$ m/W is the maximum of the gain [16]. These are typical values that depend on the fiber type as well as on the center wavelength.

The main difference between SRS and SBS is that the latter generates signals propagating counter to the initial (pump) signal. SBS is therefore significant in bidirectional transmission systems where it provides for energy flow into the Stokes band, and for crosstalk. Due to the low intensity threshold it can be severely limiting in multichannel systems with narrowband channels.

5. NUMERICAL EXAMPLES

To calculate pulse-envelope propagation along nonlinear fibers, one has to use a discrete version of the nonlinear fiber equations (12)/(13). Two different algorithms were developed. The first one neglects SBS and consists of a pseudo-spectral method using fast convolutions and a central-differences approach with a second-order integration rule. The nonlinearity is calculated partly in the time and in the frequency domain whereas linear effects are calculated in the frequency domain only. This is illustrated in Fig. 3. The second algorithm is described in the next chapter.

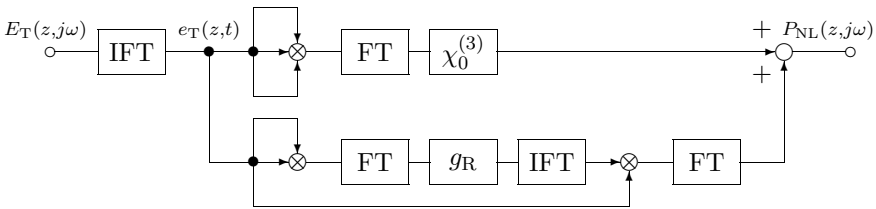


Figure 3. Calculation of the nonlinear susceptibility using fast convolution.

Using the first algorithm, calculating the propagation of a given broadband signal along a distance of 50 m with steps of 1 m and 16 k samples from the signal's spectrum takes approximately 10 min. on a PowerPC 601 machine with 66 MHz clock rate. Calculations over 100 km with 512 samples and steps of 5 m take about 15 min. on the same machine. Considering the same step width, this is almost as fast

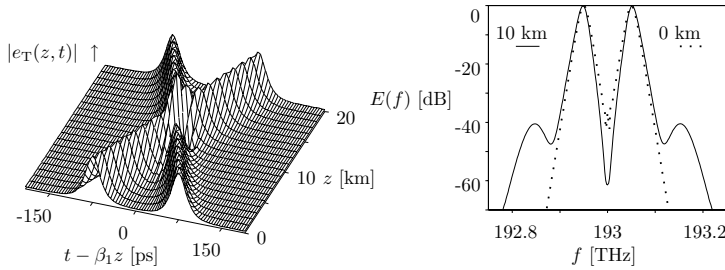


Figure 4. Crossing of two fundamental solitons and spectrum during maximum interaction (same result with both algorithms).

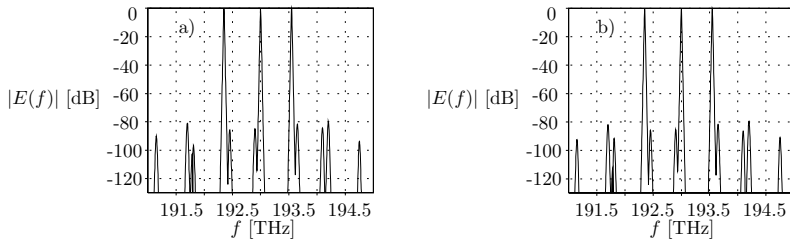


Figure 5. Spectra of FWM, $B_{\max} = 3.6$ THz. a) Fiber equations, b) NLSE.

as the same computation with the NLSE/split-step Fourier algorithm. We solved the NLSE with a symmetrized split-step Fourier algorithm [3] including third order dispersion but omitting SRS. Due to the use of a rather simple second-order finite differences algorithm for solving the fiber equations, larger step widths in the direction of propagation can be used with the split-step Fourier algorithm resulting in faster calculations.

To compare both models, we calculated the propagation of various signals of different bandwidth along ITU-T G.652 single-mode fibers. We started with single fundamental solitons of 100 ps FWHM pulse width. A quantitative comparison showed that the maximum deviation Δ of the field level of both models lies within $|\Delta| < 0.01$ dB (compared to the maximum).

Next, XPM/FWM of signals of two and three carrier frequencies was investigated. Again, fundamental solitons were used as other pulses

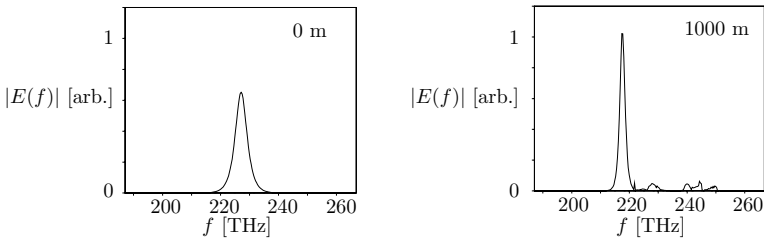


Figure 6. Spectra showing soliton self-frequency shifting.

tend to get destroyed by nonlinear interactions. As a first example Fig. 4 shows two solitons passing each other. Also shown is the spectrum calculated at the position where maximum interaction occurs. As can be seen, sidebands are generated during the interaction that vanish as soon as the pulses separate from each other. Again, both models produce very nearly the same results ($|\Delta| < 0.05$ dB) although the overall bandwidth was increased to 400 GHz.

To consider increasing bandwidth we investigated FWM effects with different channel spacings. Our simulations show that up to a bandwidth of 2.5 THz both models exhibit little deviations ($|\Delta| < 0.5$ dB). If the bandwidth is increased beyond this value, significant deviations occur that can exceed 8 dB. This is shown in Fig. 5 where an overall bandwidth of 3.6 THz is covered resulting in differences of the values of the mixing products of about 5 dB.

Next, we studied Raman effects with bandwidths beyond 5 THz. We compared modeling the Raman gain by using a single Lorentzian spectral profile [3, 7, 8, 18] to our modified Sellmeier approach (17).

As the first test of our Sellmeier approach, soliton self-frequency shifting [19] was investigated. We used a fundamental soliton of $T = 90$ fs FWHM and a peak power of 50 W. Fig. 6 shows that the center frequency of the pulse has been down-shifted nearly 15 THz within a propagation length of 1000 m. Additional SPM occurs, resulting in a slight narrowing of the pulse. A small fraction of the power density remains at the initial center frequency.

The second example of Raman interaction is energy conversion from a strong pump wave to signals located in the Stokes band of the pump. This mechanism can be observed in Raman amplifiers and with detrimental results in WDM systems with large channel spacings. Pumping of the Stokes signal is most efficient when the pump and probe signals

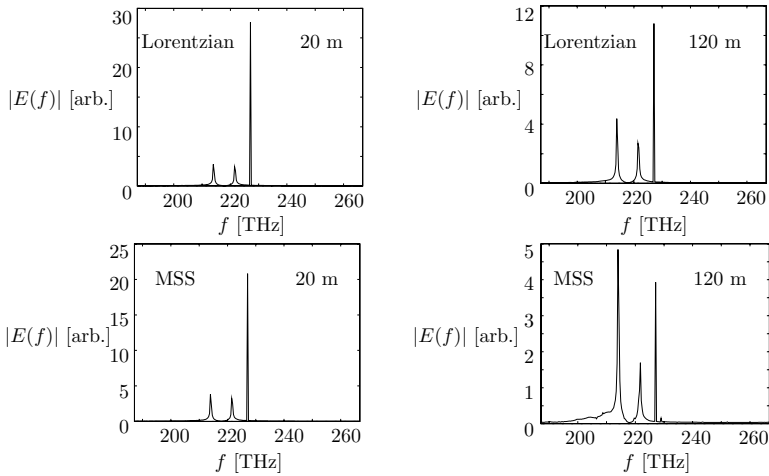


Figure 7. Raman pumping of probes spaced 5.5 and 13 THz apart from the pump. Raman gain spectrum modeled by a single Lorentzian resp. by the modified Sellmeier series (MSS) according to equation (17) and Tab. 1.

are spaced $\Delta f \approx 13$ THz apart, as this is the frequency difference where the Raman gain has its maximum, see Fig. 2. On the other hand, the Lorentzian and Sellmeier approaches differ significantly for frequency differences below 10 THz. We thus examined the pumping of two probe signals located 5.5 resp. 13 THz below the pump wave. Results of the propagation over a distance of 120 m are shown in Fig. 7. Stronger energy conversion towards lower frequencies occurs when the gain spectrum is modeled by the modified Sellmeier series according to equation (17) and Tab. 1. In this particular case the level of the $\Delta f = 13$ THz probe signal exceeds the pump after propagating over a distance of 120 m. This is caused by pumping the $\Delta f = 5.5$ THz probe signal more efficiently compared to the Lorentzian approach. This leads to even more efficient pumping of the $\Delta f = 13$ THz probe signal by the pump *and* the $\Delta f = 5.5$ THz probe signal.

Close correlation has therefore been shown between our fiber equations and the NLSE/split-step Fourier algorithm for bandwidths not exceeding 2.5 THz. The NLSE can be extended to include SRS, but this results in the need for a new algorithm and consequently slower calculations as the split-step Fourier algorithm cannot be used anymore. The pseudo-spectral algorithm based on the fiber equations is

still applicable and, together with a more detailed modeling of SRS, yields fast, convenient, and precise calculations of Raman effects. However to accurately describe SBS, which produces counter propagating waves, an improved bidirectional algorithm has to be incorporated.

6. PROPOSAL OF AN EFFICIENT BIDIRECTIONAL ALGORITHM

The major approximation of the NLSE and the split-step Fourier algorithm is omitting the second derivative with respect to z . This derivative is required for the calculation of bidirectional signal propagation. The *Finite-Differences Time-Domain method* (FDTD) has been developed to directly solve Maxwell's equations in the time domain thus retaining the second derivative. The FDTD method has been used previously in nonlinear optics [11, 12]. The disadvantage is that it is a very slow method and that it requires large memory. Here we propose a new algorithm that is able to increase the simulation speed by at least a factor of 1000. This algorithm is based on Yee's algorithm [20] and additionally uses a pseudo-spectral approach.

We start by transforming the fiber equations (7)/(8) into the time domain. This yields:

$$\frac{\partial e(z, t)}{\partial z} = \mu_0 \frac{\partial h(z, t)}{\partial t} \quad (19)$$

$$\frac{\partial h(z, t)}{\partial z} = \varepsilon_0 \frac{\partial e(z, t)}{\partial t} + \frac{\partial p(z, t)}{\partial t} \quad (20)$$

For simplicity, we now neglect Raman scattering. The polarization $p(z, t)$ can then be written as:

$$\begin{aligned} p(z, t) = \varepsilon_0 \int_{-\infty}^{\infty} \chi_{\text{eff}}^{(1)}(t - \tau) e(z, \tau) d\tau + \varepsilon_0 \chi_0^{(3)} e^3(z, t) \\ + \varepsilon_0 e(z, t) \int_{-\infty}^{\infty} h_{\text{B}}(t - \tau) e^2(z, \tau) d\tau \end{aligned} \quad (21)$$

XPM and FWM between signals of anti-parallel directions of propagation is neglected to split the signals into forward (index F) and backward (index B) propagating signals that will be coupled by Brillouin scattering only. The bandpass signals can then be expressed by

the corresponding complex envelopes (index T) as follows:

$$e(z, t) = e_{\text{TF}}(z, t) e^{j(\omega_0 t - k_0 z)} + e_{\text{TB}}(z, t) e^{j(\omega_0 t + k_0 z)} \quad (22)$$

and similar for $h(z, t)$ and $p(z, t)$.

Neglecting Raman scattering and in view of

$$\begin{aligned} & \left| e_{\text{TF}}(z, t) e^{j(\omega_0 t - k_0 z)} + e_{\text{TB}}(z, t) e^{j(\omega_0 t + k_0 z)} \right|^2 \\ & = |e_{\text{TF}}(z, t)|^2 + |e_{\text{TB}}(z, t)|^2 + \text{mixed terms} \end{aligned} \quad (23)$$

the polarization in forward direction can be written as:

$$\begin{aligned} p_{\text{TF}}(z, t) &= \varepsilon_0 \int_{-\infty}^{\infty} \chi^{(1)}(t - \tau) e_{\text{TF}}(z, \tau) d\tau \\ &+ \varepsilon_0 \chi_0^{(3)} |e_{\text{TF}}(z, t)|^2 e_{\text{TF}}(z, t) \\ &+ \varepsilon_0 e_{\text{TB}}(z, t) \int_{-\infty}^{\infty} h_{\text{B}}(t - \tau) |e_{\text{TB}}(z, t)|^2 d\tau \end{aligned} \quad (24)$$

The polarization in backward direction follows by simply replacing all indices F by B, and vice versa. Now discrete equations are derived where the samples of the electric and the magnetic field are shifted with respect to each other. The resulting lattice of width Δz and Δt is shown in Fig. 8.

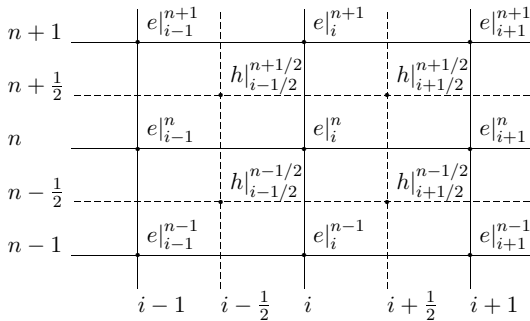


Figure 8. Lattice of the numerical algorithm [20].

Introducing discrete signals $e(i\Delta z, n\Delta t) = e|_i^n$, $h((i-1/2)\Delta z, (n-1/2)\Delta t) = h|_{i-1/2}^{n-1/2}$, $p(i\Delta z, n\Delta t) = p|_i^n$ and central differences, we obtain an algorithm for calculating the propagation of complex envelopes (again only the forward traveling part is shown):

$$h_{\text{TF}}|_{i-1/2}^{n+1/2} = h_{\text{TF}}|_{i-1/2}^{n-1/2} + \frac{1}{\mu_0} \frac{\frac{1}{\Delta z} - j\frac{k_0}{2}}{\frac{1}{\Delta t} + j\frac{\omega_0}{2}} (e_{\text{TF}}|_i^n - e_{\text{TF}}|_{i-1}^n) \quad (25)$$

$$e_{\text{TF}}|_i^{n+1} = e_{\text{TF}}|_i^n - \frac{1}{\varepsilon_0} \left(p_{\text{TF}}|_i^{n-1} - p_{\text{TF}}|_i^n - \frac{1}{\Delta z} - j\frac{k_0}{2} \left(h_{\text{TF}}|_{i+1/2}^{n+1/2} - h_{\text{TF}}|_{i-1/2}^{n+1/2} \right) \right) \quad (26)$$

The polarization can be computed using fast convolution:

$$\begin{aligned} p_{\text{TF}}|_n^i &= e^{-j\omega_0 i \Delta t} \varepsilon_0 \mathcal{I} \mathcal{F} \mathcal{F} \mathcal{T} \left\{ X_{\text{eff}}^{(1)}(jk\Delta\omega) \mathcal{F} \mathcal{F} \mathcal{T} \left\{ e_{\text{TF}}(n\Delta z, k\Delta t) \right\} \right\} \\ &+ \varepsilon_0 \chi_0^{(3)} |e_{\text{TF}}(n\Delta z, i\Delta t)|^2 e_{\text{TF}}(n\Delta z, i\Delta t) \\ &+ \varepsilon_0 e_{\text{TB}}(n\Delta z, i\Delta t) \\ &\cdot \mathcal{I} \mathcal{F} \mathcal{F} \mathcal{T} \left\{ X_{\text{SBS}}^{(3)}(jk\Delta\omega) \mathcal{F} \mathcal{F} \mathcal{T} \left\{ |e_{\text{TB}}(n\Delta z, k\Delta t)|^2 \right\} \right\} \quad (27) \end{aligned}$$

Considering complex envelopes and using fast convolutions leads to a fast numerical algorithm that is superior to common FDTD methods. By extracting the rapidly varying optical carrier the simulation time can be reduced by at least a factor of 1000. One problem of this algorithm is that it may require very large RAM in the order of 2 Gb. As a consequence, we only were able to carry out some very simple tests showing that the algorithm works. Extensive studies of the algorithm can be done when large-RAM workstations become more available in the near future.

7. CONCLUSIONS

We have presented a full-signal approach for describing broadband pulse-envelope propagation in the frequency domain by means of generalized nonlinear transmission-line equations. These *nonlinear fiber*

equations use Sellmeier's series in the frequency domain instead of a truncated Taylor series for modeling linear dispersion. Raman scattering is included by a complex third-order susceptibility that is modeled using a specially modified Sellmeier series leading to an improved broadband description of Raman effects. Brillouin scattering can be accounted for in the same way provided that a numerical algorithm can handle bidirectional signal propagation.

Numerical comparisons between the nonlinear fiber equations solved by a second-order pseudo-spectral method and the NLSE solved by a symmetrized split-step Fourier algorithm showed increasing deviations for bandwidths exceeding 2.5 THz. It was also shown that proper modeling of the Raman susceptibility by means of a modified Sellmeier series is important for the description of Raman effects between signals that are spaced 5...6 THz. Finally we showed that an efficient numerical algorithm for calculating bidirectional signal propagation can be derived based on the nonlinear fiber equations with complex envelope spectra. Given a workstation with large RAM capacities this will provide for a full-signal description of bidirectional signal propagation under nonlinear conditions.

REFERENCES

1. Spirit, D. M., and M. J. O'Mahony, *High Capacity Optical Transmission Explained*, Wiley, Chichester, 1995.
2. Barnes, S. R., J. Devos, P. M. Gabla, and B. Le Mouël, "150 years of submarine cable systems—from Morse code to cyber talk," *Alcatel Telecomm. Rev.*, 55–62, 1st quarter 1997.
3. Agrawal, G. P., *Nonlinear Fiber Optics*, Academic Press, San Diego, 2nd edition, 1995.
4. Hasegawa, A., and Y. Kodama, *Solitons in Optical Communications*, Clarendon Press, Oxford, 1995.
5. Newell, A. C., and J. V. Moloney, *Nonlinear Optics*, Addison-Wesley, Redwood City, 1992.
6. Marcuse, D., *Theory of Dielectric Optical Waveguides*, Academic Press, San Diego, 2nd edition, 1991.
7. François, P. L., "Nonlinear propagation of ultrashort pulses in optical fibers: total field formulation in the frequency domain," *J. Opt. Soc. Am. B*, Vol. 8, No. 2, 276–293, Feb. 1991.
8. Blow, K. J., and D. Wood, "Theoretical description of transient stimulated Raman scattering in optical fibers," *IEEE J. Quantum Electron.*, Vol. 25, No. 12, 2665–2673, Dec. 1989.

9. Ablowitz, M. J., D. J. Kaup, A. C. Newell, and H. Segur, "The inverse scattering transform-Fourier analysis for nonlinear problems," *Studies Appl. Math.*, Vol. 53, No. 4, 249–315, 1974.
10. Zakharov, V. E., and A. B. Shabat, "Exact theory of two-dimensional self-focusing and one-dimensional self-modulation of waves in nonlinear media," *Sov. Phys. JETP*, Vol. 34, No. 1, 62–69, Jan. 1972.
11. Taflove, A., *Computational Electrodynamics*, Artech House, Boston, 1995.
12. Joseph, R. M., and A. Taflove, "FDTD Maxwell's equations models for nonlinear electrodynamics and optics," *IEEE Trans. Antennas Propagat.*, Vol. 45, No. 3, 364–374, Mar. 1997.
13. Stoll, D., *Nichtlineare Wellenausbreitung in Single-Mode-Fasern*, VDI-Verlag, Düsseldorf, 1994.
14. Sutherland, R. L., *Handbook of Nonlinear Optics*, Marcel Dekker, New York, 1996.
15. Stolen, R. H., "Nonlinearity in fiber transmission," *Proc. IEEE*, Vol. 68, No. 10, 1232–1236, Oct. 1980.
16. Stolen, R. H., "Nonlinear properties of optical fibers," in *Optical Fiber Telecommunications*, S. E. Miller and A. G. Chynoweth, Eds., 125–150. Academic Press, San Diego, 1979.
17. Kim, K. S., R. H. Stolen, W. A. Reed, and K. W. Quoi, "Measurement of the nonlinear index of silica-core and dispersion-shifted fibers," *Opt. Lett.*, Vol. 19, No. 4, 257–259, Feb. 1994.
18. Stolen, R. H., J. P. Gordon, W. J. Tomlinson, and H. A. Haus, "Raman response function of silica-core fibers," *J. Opt. Soc. Am. B*, Vol. 6, No. 6, 1159–1166, June 1989.
19. Mitschke, F. M., and L. F. Mollenauer, "Discovery of the soliton self-frequency shift," *Opt. Lett.*, Vol. 11, No. 10, 659–661, Oct. 1986.
20. Yee, K. S., "Numerical solution of initial boundary value problems involving Maxwell's equations in isotropic media," *IEEE Trans. Antennas Propagat.*, Vol. AP-14, No. 4, 302–307, Apr. 1966.